WILEY

Effects of soil–structure interaction on the design of tuned mass damper to control the seismic response of wind turbine towers with gravity base

Kaoshan Dai[1,2] | Hai Huang[2] | Yang Lu[2] | Jiayao Meng[3] | Zhenxi Mao[3] | Alfredo Camara[4]

[1]MOE Key Laboratory of Deep Underground Science and Engineering, College of Architecture and Environment, Sichuan University, Chengdu, China

[2]Department of Civil Engineering and Institute for Disaster Management and Reconstruction, Sichuan University, Chengdu, China

[3]Department of Disaster Mitigation for Structures, Tongji University, Shanghai, China

[4]School of Mathematics, Computer Science and Engineering, City, University of London, London, UK

Correspondence
Yang Lu, Department of Civil Engineering and Institute for Disaster Management and Reconstruction, Sichuan University, Chengdu 610065, China.
Email: yang.lu@scu.edu.cn

Abstract

This paper studies the effect of soil–structural interaction (SSI) on gravity-based wind turbine towers equipped with tuned mass dampers (TMDs) subjected to earthquake loading. A small-scale shaking table test of wind turbine towers with TMD was conducted, and the results showed that using TMD designed considering SSI resulted in larger vibration suppression. A simplified analytical numerical model was developed for SSI analysis considering TMD. The effect of soil site class and the earthquake intensity on the response reduction efficiency of the TMD was also discussed using the simplified model. It is concluded that the TMD efficiency depends not only on the soil stiffness but also on the characteristics of the applied ground motions, both of which are affected by the site classes and earthquake intensity levels. Moreover, the peak acceleration ratio (PAR), the root mean square acceleration ratio (RAR), the peak displacement ratio (PDR), and the root mean square displacement ratio (RDR) of the top of the wind turbine tower were obtained with and without TMD for different earthquake intensities and sites. These parameters can be used as references for the rational selection of TMD parameters considering SSI.

KEYWORDS

response reduction efficiency, soil–structural interaction, TMD, wind turbine tower

1 | INTRODUCTION

The world has witnessed a fast growth of wind energy over the past few decades. The worldwide wind capacity reached 600 GW by the end of 2018, with over 9.8% growth rate of total installed capacity since 2012.[1] Wind farms are widely deployed in North America and Asia; some of them constructed in high-risk seismic zones.[1] Therefore, the importance of considering seismic hazards in the design and assessment of wind turbine tower has led to an increasing research interest on the topic,[2–5] along with provisions for seismic loading included on wind turbine design guidelines.[6,7] To improve the efficiency in the generation of electricity from the wind, large-diameter rotors and thin wall slender towers are usually adopted in current designs, which are vulnerable to external excitations such as wind and seismic actions during their lifetime. These excitations can lead to excessive vibrations in the wind turbine blades and the tower, resulting in a reduction of the electricity generation or even in the failure of the blades or the tower.[8,9] Moreover, as wind turbine towers become taller, their safety and serviceability may be considerably reduced.

Therefore, it is of great significance to develop vibration suppression techniques that protect wind turbines from these hazards and improve the overall dynamic performance of the structure.

In response to these challenges and design trends, extensive research has been carried out on various vibration control devices to mitigate the wind turbines vibrations.[10] In general, these devices can be grouped into two categories: passive control systems[11-21] and active or semi-active control systems.[22,23] Active control systems are usually more expensive and less robust as they require external power sources[10] that may not be available in the event of a power shortage. Contrary to active control systems, passive control systems need no external power, and they are widely adopted in different engineering application. Among all the devices used to control wind turbine tower, tuned-type dampers are well-established and commonly used in industry, and they received most of the attention in the literature.[11-21] Murtagh et al.,[11] Lackner and Rotea,[12] and Stewart and Lackner[13] suggested using tuned mass dampers (TMDs) for the vibration control of wind turbines; Ghaemmaghami et al.[14] suggested annular tuned liquid dampers (TLDs), and Chen et al.[15] suggested spherical TLDs; Colwell and Basu,[16] Mensah and Dueñas-Osorio,[17] and Chen et al.[18] proposed tuned liquid column dampers (TLCDs); Chen and Georgakis[19] developed a rolling ball damper; Zhang et al.[20] introduced a ball vibration absorber; Zuo et al.[21] proposed using multiple tuned mass dampers (MTMDs); Zhao et al.[24] developed a novel scissor-jack braced viscous damper; Zhang et al.[25] proposed using tuned parallel inerter mass system (TPIMS). In all the cases, the results showed the effectiveness of the proposed dampers in the mitigation the wind turbine tower vibrations.

The accurate prediction of the seismic response of wind turbines is of great significance for maintaining and achieving the right balance between safety and economic efficiency. Underpredicting the seismic hazard may result in significant damage or even failure of the wind turbine, causing great economical loss and social consequences. On the other extreme, overestimating the seismic hazard may lead to high economical and environmental costs of wind turbine farms, hindering the growth and expansion of wind power. In this regard, considering the soil–structure interaction (SSI) is an important factor in the accurate evaluation of the seismic response of tall and slender structural systems like wind turbines.[26] Bazeos et al.[2] firstly studied the influence of SSI in wind turbines by introducing a set of linear springs and dashpots. The results from eigenvalue analysis showed that the fundamental frequency was significantly lower for the SSI system, which further influences the dynamic behavior of wind turbines. Similar results from other numerical[27-29] and experimental[30,31] studies confirmed the significant influence of SSI on the dynamic performance of wind turbine towers. Besides, the soil characteristics and its flexibility were also found to be of high relevance by other researches.[32,33] Consequently, ignoring the SSI in the design tuned-type dampers for wind turbines may result in detuning problems.

The objective of this study is to illustrate the influence of the SSI in the design of TMDs for wind turbines with gravity base under earthquake actions. In order to highlight the SSI effect on the parameter design of TMD, a series of small-scale shaking table tests of wind turbine towers with soil and TMDs were conducted. The experimental results confirmed that TMDs designed considering SSI were more efficient in the vibration reduction compared to those designed with a fixed-base assumption. To further discuss the effect of SSI on the TMD efficiency, a simplified numerical model was developed, which was validated by the experimental work. This model is used to perform a parametric study of the effect of the soil site class and the earthquake intensity. Based on these results, suggestions are made on the selection of TMD parameters for the optimum seismic design of wind turbine towers on flexible soils.

2 | EXPERIMENTAL STUDY ON SSI EFFECTS

2.1 | Prototype of wind turbine

A 1.5-MW capacity three-bladed horizontal-axis wind turbine with a rotor of 70-m diameter is considered in the present study; the structure is illustrated in Figure 1. This wind turbine is representative of many wind turbines currently in operation, and it has been wildly constructed in wind farms in the southeast coast of China since the early 2000s. It was designed as Class 2a according to IEC 61400[7] with no explicit considerations of seismic provisions.

The wind turbine tower is a 61.8-m-high thin-wall tapered tubular steel structure. The outer diameter ranges from 4035 mm at the base to 2955 mm at the top. The shell wall thickness varies from 25 mm at the base to 14 mm at the top, with a minimum of 10 mm near the top. The entire tower is composed of 22 segments that are welded together and is preassembled into three sections connected by bolts and heavy circular flanges for transportation and installation purposes.

The wind turbine foundation is designed by expanding circular concrete platform with a total height of 2.825 m. It consists of a cylindrical socket to which the base of the steel tower is anchored and a slab footing with the shape of a truncated cone. The socket has a 5.5-m diameter and 1.142-m height, while the footing has a diameter varying from 21.8 m at the base to 5.5 m at the top and a height of 1.583 m.

The wind turbine tower is made of generic grade S355 mild steel with yield stress $f_{y,k}$ = 355 MPa, elastic modulus E_t = 200 GPa, Poisson's ratio v_σ = 0.3, and density ρ_t = 7850 kg/m^3. The wind turbine foundation is designed of reinforced concrete with concrete grade C30/37 according to BS EN 206[34] at the socket and grade C20/25 at the footing. The mass of the supporting tower is 91 tones approximately, while the nacelle at the tower top is about 60 tones, and the blades are about 30 tones. The mass of the foundation is 400 tones approximately.

FIGURE 1 Geometry of the wind turbine tower and its foundation (units in mm)
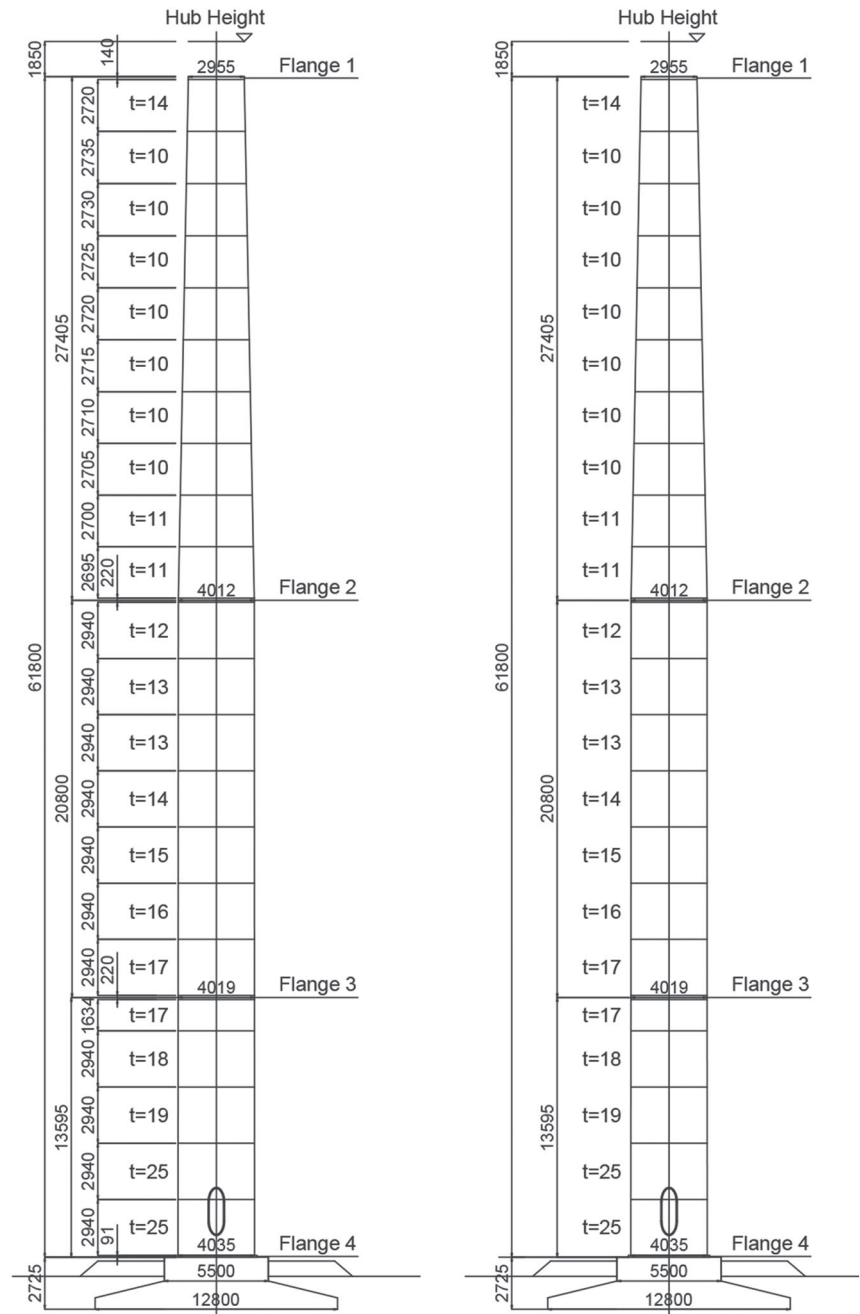
2.2 | Shaking table test model design

A small-scale shaking table test was performed to investigate and to validate the efficiency of TMD considering SSI effect. The shaking table facility used in this study consists of a 610 × 460 mm platform with a bearing capacity of 15 kg. The table is able to move in a single horizontal direction with a 400-W hydraulic servo system. The operational frequency is up to 20 Hz. Considering the size and the capacity of the shaking table, a 1/100-scale model of the prototype was designed and built for the test based on the similarity relationships shown in Table 1.[35]

It is difficult to manufacture the small-scaled model in full detail because the wind turbine prototype is a tapered thin-wall structure with variable outer diameter and wall thickness. Therefore, an equivalent simplified model was developed in the design process. Bazeos et al.[2] and Lavassas et al.[3] established a simplified multi-degree of freedom (MDOF) models for dynamic analysis consisting of a cantilever beam with distributed tower mass and a lumped mass at the top representing the blades and the nacelle. This simplified model was further validated by Prowell et al.[4] in numerical and experimental studies, and it was adopted here. Since the first vibration mode of wind turbine plays a dominant role in the dynamic response, the fundamental frequency and the first vibration mode shape calculated from the mass and stiffness matrices of the MDOF model should correspond to the parameters of wind turbine prototype. The dynamic properties of wind turbine prototype were measured on-site

Parameters	Similarity relationship	Scaling ratio (model/prototype)
Length	S_l	1/100
Horizontal displacement	S_l	1/100
Rotation	$S_\theta = S_\sigma/S_E$	1
Elastic modulus	S_E	0.3495
Stress	$S_\sigma = S_E$	0.3495
Strain	$S_\varepsilon = S_\sigma/S_E$	1
Density	$S_\rho = S_\sigma/(S_a S_l)$	11.6505
Mass	$S_m = S_\sigma S_l^2/S_a$	1.16505×10^{-5}
Poisson's ratio	-	1
Concentrated load	$S_F = S_\sigma S_l^2$	3.49515×10^{-5}
Line load	$S_{ql} = S_\sigma S_l$	0.0035
Surface load	$S_{qs} = S_\sigma$	0.3495
Moment	$S_M = S_\sigma S_l^3$	3.495×10^{-7}
Time	$S_t = S_l^{0.5} S_a^{-0.5}$	0.0577
Frequency	$S_f = S_l^{-0.5} S_a^{0.5}$	17.3205
Velocity	$S_v = (S_a S_l)^{0.5}$	0.1732
Acceleration	S_a	3

TABLE 1 Scaling ratios of the test model

by Dai et al.[36,37] Based on these results, the detailed parameters of the MDOF model were defined. A 618-mm-long thin-wall hollow aluminum tube with overall stiffness similar to the ideal wind turbine tower model of the prototype was used to represent the tower, while a concentrated mass at the top of the model was calculated and designed so that the model has a first mode satisfying the similarity criteria. The design of the blades, including the airfoil section, the chord length, and twist angle, was carefully considered for a subsequent study. Only parked conditions for the blades were considered in this study.

The foundation was represented by a truncated-conic plate made of lead with a total height of 28 mm. It has a diameter of 128 mm at the base and 55 mm at the top. The compacted soil around the foundation was poured in a containment box. As the seismic excitations were inputted in one direction, the soil box was designed in a rectangular shape to meet the shaking table capacity. To reduce the wall boundaries effects caused by wave reflection on the boundary, a flexible container was designed and built for the test. The ratio of the soil box length to the foundation diameter is 5. A rubber membrane with 2-mm thickness and a reinforcing mesh were used to provide lateral support for the soil. Further details about the soil containment box can be found in Lu et al.[38] A synthetic model soil with light weight[39] was employed for the test. The soil was prepared by mixing sawdust and sand to represent fine sand conditions. The sawdust-to-sand mass ratio is 1:2.5. A series of cyclic triaxial tests were carried out in the laboratory to verify that the soil material complies well with the similitude relations and that it reproduces the dynamic properties of the prototype soil conditions around the tower foundation.[40] For the testing with fully fixed base conditions, a steel plate with a diameter of 120 mm and a thickness of 20 mm was used to fix the model to the shaking table. The characteristics of the model are summarized in Table 2.

2.3 | TMD properties

Due to the structural configuration of the wind turbine, with a slender tower supporting a large mass on top, it is mainly controlled by the first vibration mode, regardless of the SSI. Therefore, the TMDs were designed to control the contribution of the first vibration mode to the seismic response of the structure.

Two TMDs were designed for the shaking table test model by tuning the frequency and damping ratio of the damper using the mass and frequency ratios, denoted by $\bar{m}$ and f, respectively. The ratio of f, representing the damper frequency divided by the fundamental frequency of vibration of the main structure, and the damping ratio of the damper ξ_d were calculated according to the optimum tuning proposed in Tsai et al.[41]:

$$f = \frac{\sqrt{1-0.5\bar{m}}}{1+\bar{m}}, \tag{1}$$

$$\xi_d = \sqrt{\frac{3\bar{m}}{8(1+\bar{m})(1-0.5\bar{m})}}, \tag{2}$$

TABLE 2 Technical parameters of the model

Parts	Parameters	Value
Tower	Material	Aluminum
	Height	618 mm
	Thickness	1.5 mm
	Outer diameter	22.0 mm
	Inner diameter	19.0 mm
	Mass	205.50 g
Blades	Material	Steel
	Mass	371.80 g
Nacelle	Material	Steel
	Mass	1816.90 g
Foundation	Material	Lead
	Height	28 mm
	Mass	1679.00 g
	Diameter at the top	55 mm
	Diameter at the base	128 mm
Soil box	Overall dimensions (L × W × H)	640 × 150 × 100 mm

where $\bar{m}$ denotes the ratio of the damper mass to the main system mass excluding foundation mass. The first TMD (TMD A) was designed without considering SSI, while the second one (TMD B) was designed accounting for SSI. Both TMDs were designed using Equations 1 and 2. While TMD A was designed based on the damping ratio and frequency of the fixed-base systems, TMD B was designed based on the parameters of the SSI systems. The mass ratio of both TMDs was set to $\bar{m}$ = 0.05, and their detailed parameters are shown in Table 3. Two springs with different diameter, length, and pitch (which is the distance in between the consecutive helical spring coils) were designed to provide the required stiffness. As the calculated damping of the TMD was very difficult to manufacture in the small dimension required, a device generating eddy currents was used in the TMD to produce the desired damping.[42] The simplified eddy current damping model of the TMD is shown in Figure 2.

A conductor plate with a thickness of t = 2 mm and a resistivity of $\rho_r = 1.75 \times 10^{-8}$ $\Omega \cdot m^2$/m (which is calculated as the resistance multiplied by the cross-sectional area and then divided by the length of conductor plate, considering a temperature of 20°C) is positioned beneath a permanent magnet with dimensions $a \times b$ = 10 × 22 mm and 10 × 15 mm for TMD A and TMD B, respectively. The distance between the magnet and the conductor plate is 5 mm, to create a uniform magnetic field with induction intensity B = 1.24 T. When the conductor plate moves horizontally with a velocity of V, an electromotive force is generated in the conductor plate. The electromotive force of a differential of volume with dimensions $da \times b \times t$:

$$d\varepsilon = BVb, \tag{3}$$

TABLE 3 Parameters of the tuned mass dampers

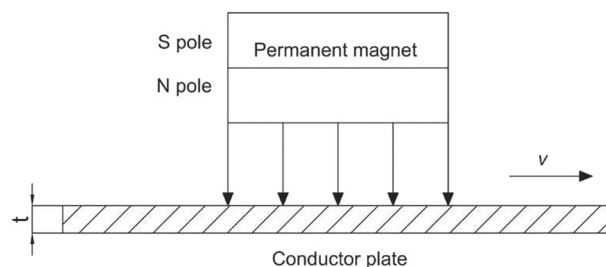| Damper	$\bar{m}$	Mass (kg)	Circular frequency (rad/s)	Stiffness (N/m)	Damping coefficient (N/[m/s])
TMD A (without SSI)	0.05	0.1197	41.53	206.47	1.35
TMD B (with SSI)	0.05	0.1197	29.73	93.58	0.91

FIGURE 2 Simplified model of eddy current damping

FIGURE 3 TMD based on eddy current used in this work

and the differential resistor,

$$dR = \frac{\rho_r b}{t da}, \tag{4}$$

give the eddy current intensity of this differential:

$$dI_n = \frac{d\varepsilon}{2dR} = \frac{BVtda}{2\rho_r}. \tag{5}$$

The force generated from the current in the differential volume element crossing the magnetic induction line can be calculated as follows:

$$dF = BbdI_n = \frac{B^2 bda}{2\rho_r}. \tag{6}$$

By integrating dF in the volume of the conductor plate, the resultant force can be calculated as follows:

$$F = \frac{B^2 Vabt}{2\rho_r}. \tag{7}$$

The theoretical eddy current damping coefficient is as follows:

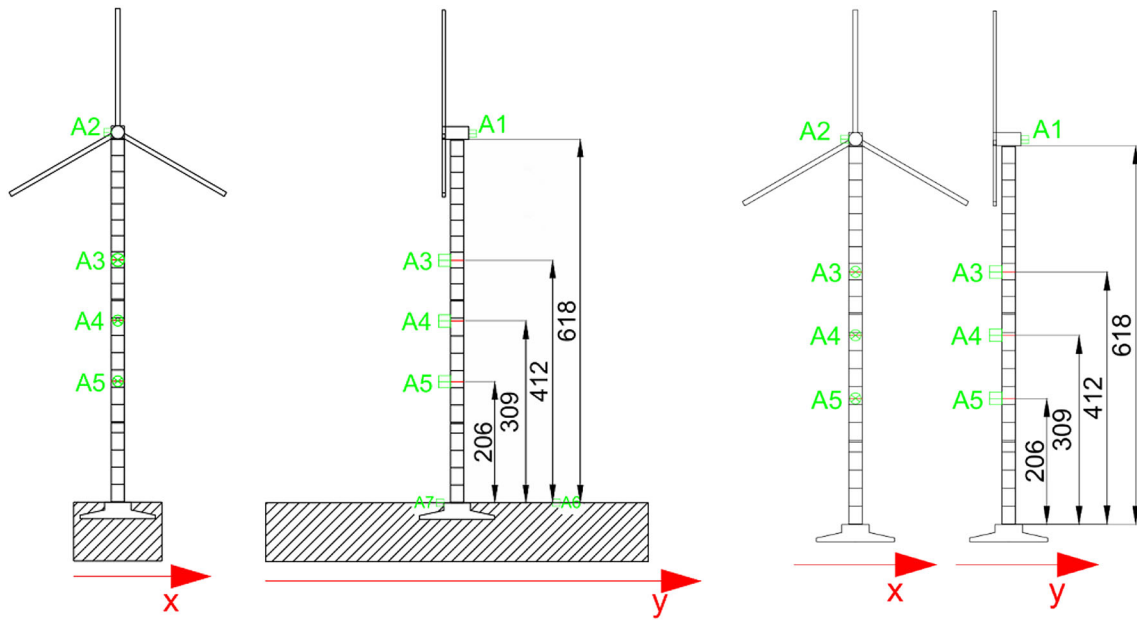$$c_{ec} = k_c \frac{F}{V} = k_c \frac{B^2 abt}{2\rho_r}, \tag{8}$$

FIGURE 4 Position of the sensors (units in mm)

FIGURE 5 Test model configuration

where $k_c = 0.7$ is a modifying coefficient to account for the fact that the actual magnetic field is not perfectly uniform. Figure 3 shows the physical TMD model designed for this study.

2.4 | Test setup and program

Two accelerometers (A1 and A2) were installed at the top of the tower to measure the response of the model in the two horizontal directions during the tests: x (side–side) and y (fore–aft). Three accelerometers (A3, A4, and A5) were installed at the middle point of the tower to measure the response in y direction as shown in Figure 4. Two accelerometers (A6 and A7) were positioned at the soil surface to obtain the response of the ground in y direction. The test model configuration is shown in Figure 5.

Two typical ground motion time histories were adopted as inputs in the test: 1940 Imperial Valley and 1952 Kern County. The earthquake records were selected from the Pacific Earthquake Engineering Research (PEER) database of strong ground motions.[43] The acceleration values and the duration of the motions were modified based on the similarity relations. The ground motion is applied in the y direction.

2.5 | Test results

Free vibration tests were firstly conducted to obtain the dynamic properties of the model. The fundamental frequency of the model with fixed-based conditions in the y direction was 21.36 rad/s from tests results. The theoretical fundamental frequency of the test model was calculated from the prototype frequency and similarity relationship as 21.77 rad/s. The relative error is only 1.86%. The fundamental frequencies of the model with flexible soil were 13.54 and 14.86 rad/s, respectively. The damping ratio of the test model was measured to be 1.263% and 8.787% for fixed-based condition and flexible soil conditions, respectively.

For fixed-based conditions, the acceleration responses at the top of the test model with and without vibration control with TMD A (ignoring SSI in its design) were compared to study the vibration suppression efficiency of TMD designed without SSI. The comparison of the tower top acceleration responses under different ground motion inputs is shown in Figure 6. The ground motions recorded by the ElCentro (ELC) station in the 1940 Imperial Valley earthquake and the Taft station in the 1952 Kern County earthquake were used. The vibration reduction coefficients of peak value and the root mean square (RMS) values over the entire time history are reported in Table 4. If we define $\ddot{X}_i$ to be acceleration at time i, the RMS of acceleration, denoted $\ddot{X}_{RMS}$, is given by Equation 9.

$$\ddot{X}_{RMS} = \sqrt{\frac{\sum_{i=1}^{N} \ddot{X}_i^2}{N}}, \tag{9}$$

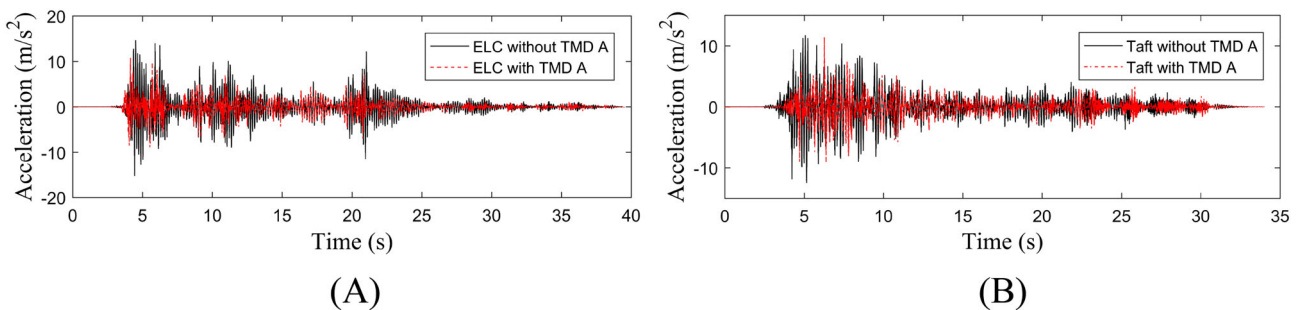where N represents the number of time points in the time history.

FIGURE 6 Comparison of acceleration at the tower top of the model with fixed-base conditions and with or without TMD A: (A) 1940 Imperial Valley earthquake; (B) 1952 Kern County earthquake

	Imperial Valley 1940	Kern County 1952
Peak value coefficient	29.18%	8.94%
RMS value coefficient	42.94%	35.66%

TABLE 4 Vibration reduction coefficients at the tower top of the model with fixed-base conditions and TMD A
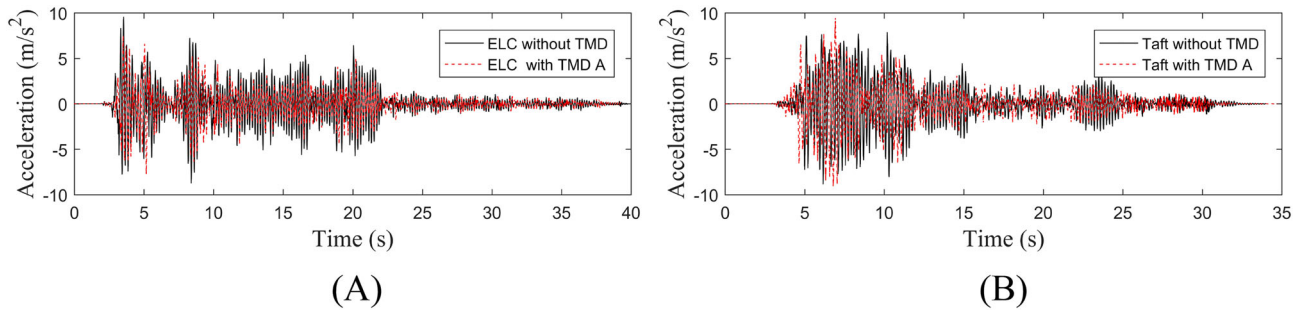
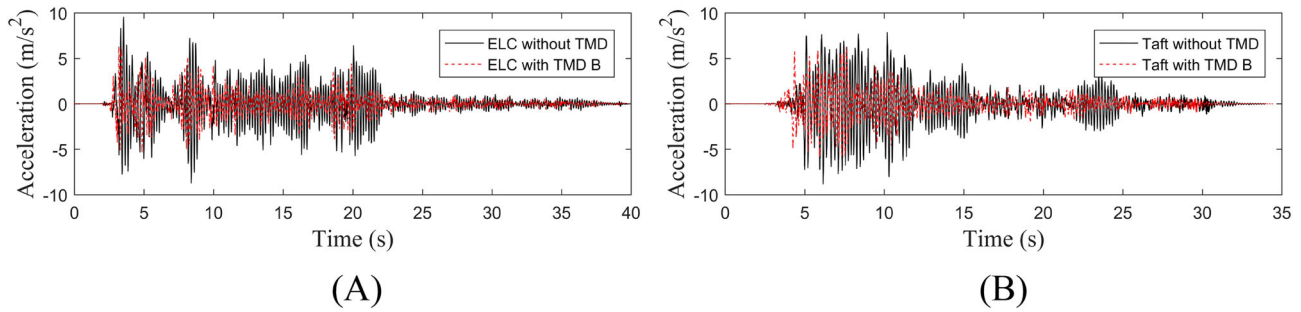**FIGURE 7** Comparison of the tower top accelerations with TMD A: (A) 1940 Imperial Valley; (B) 1952 Kern County

FIGURE 8 Comparison of the tower top accelerations with TMD B: (A) 1940 Imperial Valley; (B) 1952 Kern County

TABLE 5 Vibration suppression coefficients of TMD A and TMD B in the model with flexible soil at the base

		Imperial Valley 1940	Kern County 1952
TMD A	Peak value coefficient	19.31%	−6.56%
	RMS value coefficient	26.61%	16.09%
TMD B	Peak value coefficient	32.94%	29.25%
	RMS value coefficient	41.92%	42.54%

TABLE 6 Dynamic stiffness and dashpot coefficients

	Lateral	$K_s = \frac{8GR_f}{2-v}\left(1+0.5\frac{R_f}{H_s}\right)$
K_s	**Rocking**	$K_r = \frac{8GR_f}{3(1-v)}\left(1+0.17\frac{R_f}{H_s}\right)$
k	Lateral	0.99
	Rocking	0.98
C_R	Lateral	$C_R = 0$ at $f_b < \frac{3}{4}f_s$
		$C_R = \rho_s V_S A_f$ at $f_b > \frac{4}{3}f_s$
		At intermediate frequencies : interpolate linearly
		$f_s = \frac{V_s}{4H_s}$ $V_S = \sqrt{\frac{G}{\rho_s}}$
	Rocking	$C_R = 0$ at $f_b < f_c$
		$C_R = \rho_s V_{La} I_b$ at $f_b > f_c$
		$V_{La} = \frac{3.4}{\pi(1-v)}V_s$ $f_c = \frac{V_{la}}{4H_s} = \frac{3.4}{\pi(1-v)}V_s$

Note: G = shear modulus of soil; ρ_s = mass density of soil; v = Poisson's ratio of soil; H_s = soil depth; R_f = foundation radius; f_s = the natural fundamental frequency of the stratum corresponding to the "shearing" modes of vibration; f_c = the natural fundamental frequency of the stratum corresponding to the "compressing" modes of vibration; f_b = excitation frequencies; V_s = soil shear wave velocity; V_{La} = apparent compression wave velocity of soil; A_f = foundation area; I_b = foundation moment of inertia.

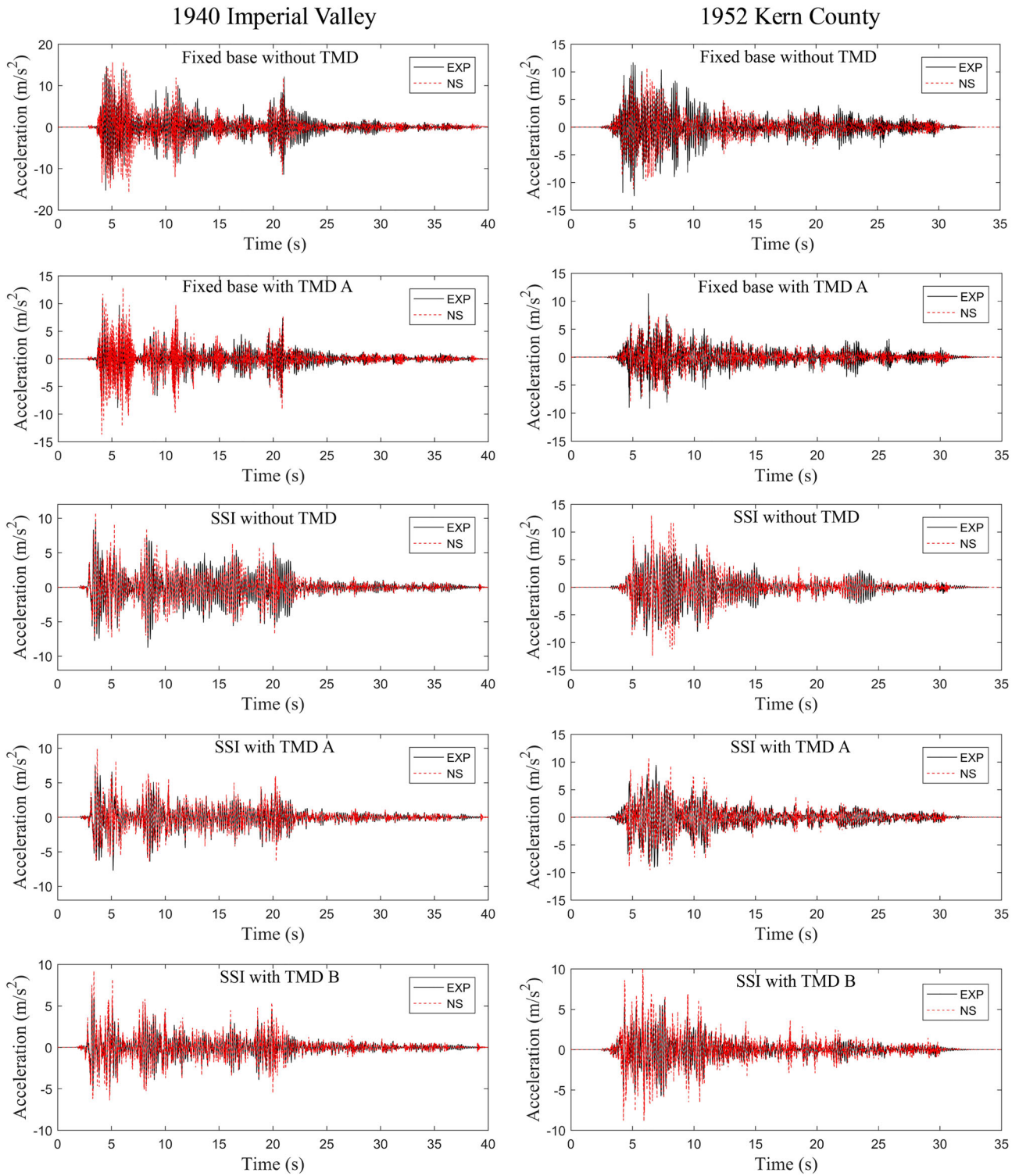## 1940 Imperial Valley   ## 1952 Kern County

FIGURE 9 Comparison of acceleration responses at the tower top in the experimental (EXP) and the numerical (NS) results

In the model with soil, two types of TMDs were designed, with and without considering SSI (TMD A and TMD B, respectively). The acceleration response at the tower top was compared to the response of model without vibration control. The results are shown in Figures 7 and 8 for TMD A and TMD B, respectively. The vibration suppression coefficients with the two TMDs were calculated and compared in Table 5.

Table 5 shows that the TMD A can reduce the vibrations on the tower top effectively when the tower is fully fixed at its base, which corresponds to an idealized foundation in rock. However, if the wind turbine is founded in soil, the flexibility of its foundation reduces the efficiency of

TMD A. The TMD B, which accounts for SSI in its design, is significantly more efficient than TMD A in these conditions, both in terms of peak values and RMS values.

3 | DEVELOPMENT OF A SIMPLIFIED NUMERICAL MODEL FOR WIND TURBINES WITH TMDS CONSIDERING SSI

A simplified wind turbine tower model is established considering both the effects of TMD and SSI. The model will be validated against experimental data shown in the previous sections, and it will serve as a practical tool for the evaluation of the seismic response reduction efficiency of TMDs in wind turbines located on different site classes in Section 4.

3.1 | Model establishment

The tower can be modeled using a number of planar Euler beams that consider shear deformation. The dynamic equation of motion of the tower can be written as follows:

$$M\ddot{X} + C\dot{X} + KX = MI_e\ddot{u}_g(t),$$ (10)

where M is the mass matrix of the structure; C is the damping matrix; K is the stiffness matrix; I_e is the influence coefficient that relates the degrees of freedom of the structure with those of the earthquake; X is the displacement vector of structural deformation shape; $\dot{X}$ is the velocity vector; $\ddot{X}$ is the acceleration vector; $\ddot{u}_g(t)$ is the ground acceleration.

The stiffness matrix of a shear-deformable beam element and its mass matrix can be found in Du et al.,[44] and they are provided in Appendix A for convenience. Consistent mass matrices were adopted to model the mass of the tower, while lumped masses were assigned to the top and the bottom of the tower in order to take into account the combined nacelle and blade masses, as well as the foundation mass, respectively. An extra DOF was introduced to accommodate the mass, stiffness, and damping coefficient of the TMDs. The foundation sway-rocking response at the tower base was simulated using discrete springs and dashpots that represent the stiffness and damping characteristics of the foundation motion. The stiffness and damping coefficients at the tower base are determined using the following formulae[45]:

$$\bar{K}_s = K_s k,$$ (11)

$$\bar{C}_s = C_R + \frac{2\bar{K}_s}{\omega}\beta_0,$$ (12)

where $\bar{C}_s$ is the foundation damping; $\bar{K}_s$ is the foundation dynamic stiffness; K_s is the foundation static stiffness; k is the dynamic stiffness coefficient; ω is calculated as the circular frequency of vibration corresponding to the fundamental mode of vibration of the system; β_0 is the soil hysteretic damping ratio; C_R is the foundation radiation damping. These parameters can be calculated using Table 6, taken from Gazetas.[45]

Ten beam elements were used to model the tower, with an element length of 61.8 mm. The Newmark-β method was used to solve Equation 10 with a time step of 1/265 s. A Rayleigh damping model distribution was considered. It was based on a damping ratio 1.263% (measured in the lab test model) assigned to the first and the second modal frequencies of vibration of the tower.

3.2 | Model validation

In order to compare the results of the experiments (EXP) and the numerical simulations (NS), the two sets of data are plotted together in Figure 9. Fixed-base and flexible-base models were adopted to validate the vibration properties of the wind turbine tower and the associated SSI systems, respectively. The effective shear modulus and damping ratios of the soil material used in the EXP were measured and introduced in the NS. In general, the NS results are consistent with those obtained experimentally. The peak and the RMS values of the acceleration response at the top of the tower are provided in Table 7. The averaged differences between the EXP and NS results are about 20% and 10% for the peak and for the RMS accelerations, respectively. The peak values only reflect the instantaneous response, and the RMS values take into account the entire response history. Consequently, the RMS may be more meaningful for serviceability checks, such

TABLE 7 Peak and root mean square (RMS) values of tower top accelerations, units in m/s^2

| | | Fixed base | | | | With soil at the base | | | |
| | | Test model | | Numerical model | | Test model | | Numerical model | |
		Peak	RMS	Peak	RMS	Peak	RMS	Peak	RMS
Imperial Valley 1940	Without TMD	14.6730	2.0454	15.8205	2.2668	9.5758	1.8363	10.7909	1.5546
	With TMDA	10.8320	1.1671	13.7014	1.5849	7.7264	1.3476	9.8694	1.3176
	With TMDB	N/A	N/A	N/A	N/A	6.4216	1.0664	9.1984	1.1720
Kern County 1952	Without TMD	12.4913	1.8128	11.2097	1.6678	8.8564	1.9803	13.0332	1.8739
	With TMDA	11.3747	1.1664	7.9993	1.1886	9.4378	1.6617	10.8232	1.5033
	With TMDB	N/A	N/A	N/A	N/A	6.2656	1.1378	10.0770	1.3286

as the study of the operation safety of the machinery in the nacelle. But the peak is also important for ultimate limit state checks, for example, to study the structural capacity of the tower. In the case of the fixed-base tower with TMD A subjected to the 1952 Kern County earthquake, the relative difference between the EXP and NS results of the peak acceleration is 40.22%, whereas the difference of the RMS is only 1.87%. When considering SSI, the EXP-NS difference of RMS accelerations of the tower, in the case of the 1940 Imperial Valley earthquake with TMD A, is only 2.28%. However, there are some cases in which the experimental RMS accelerations with SSI are somewhat different from those obtained using the NS by more than 10%. The reason for the error may be due to the beam model (used in NS) simplification, which is 2D while the lab test model is 3D. In addition, the foundation model (used in NS) is an approximation of the real soil behavior. The differences between the numerical and test results may also related to measurement errors, manufacture imperfection of the TMDs, and so on.

3.3 | Frequency response analysis

In order to explore the effectiveness of the TMDs for different vibration frequencies, the response transfer functions (TFs) were calculated and presented in Figure 10, where $\ddot{X}_t$ and $\ddot{X}_g$ represent the absolute acceleration amplitude of the top of the wind turbine tower and ground acceleration amplitude, respectively, and X_t represents the relative displacement amplitude response of the top of the wind turbine tower. Figure 10A shows the TF between the ground acceleration and the tower top acceleration, and Figure 10B illustrates the TF relating ground acceleration to tower top displacement relative the ground. The first peaks in the TFs of the wind turbines on fixed or flexible bases are associated with the
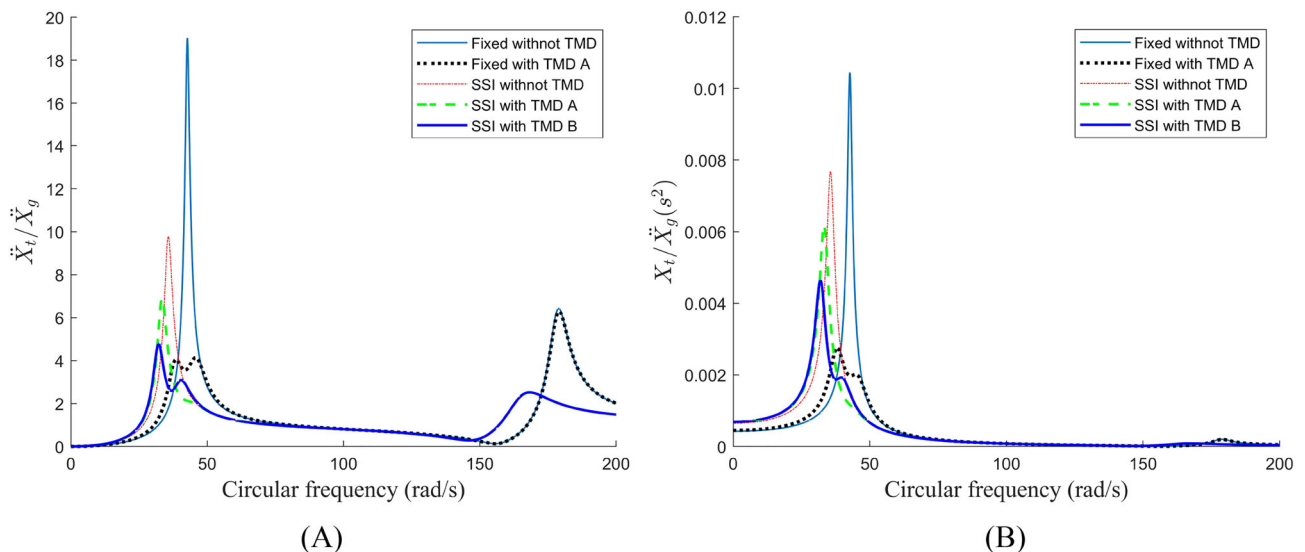
FIGURE 10 Transfer functions of wind turbine tower under different cases: (A) ground-to-tower top absolute acceleration and (B) ground acceleration-to-tower top relative displacement

fundamental frequencies of the corresponding structural systems as they were measured in the EXP. Compared with the wind turbine without TMDs, the response reduction efficiency of the peak accelerations at the tower top are 78.46%, 29.42%, and 50.87% for the fixed-base system with TMD A, the SSI system with TMD A, and the SSI system with TMD B, respectively. Considering the peak displacements at the top of the tower, the efficiencies of the same TMDs are 73.38%, 19.57%, and 39.42%, respectively. These results show that the TMD response reduction efficiency is weaker for the SSI system than for the fixed-base system, and when considering SSI, using TMD B is much more effective than using TMD A. Therefore, it is verified that TMDs should be designed on the basis of the SSI system.

3.4 | Displacement response

Figure 11 shows the displacement of the top of the wind turbine tower from the NS. It can be seen that the fixed-base structure system with TMD A is the most efficient one in the reduction of the tower top displacements, followed by the structure on flexible foundation with TMD B and then by the same structure with TMD A. Table 8 shows that using TMD B (designed based on the SSI system) resulted in larger reduction of the tower top displacements than using TMD A (design based on the fixed-base system), demonstrating that SSI should be considered in the design of TMD. This also confirms the results obtained in the frequency domain.

4 | NUMERICAL STUDY ON SSI EFFECTS ON TMD DESIGN

Soil properties vary from on-site to another resulting in different ground motion characteristics and SSI features. In addition, the soil shear modulus and damping are affected by the earthquake intensity. Therefore, it is necessary to explore the combined and coupled influence of site soil
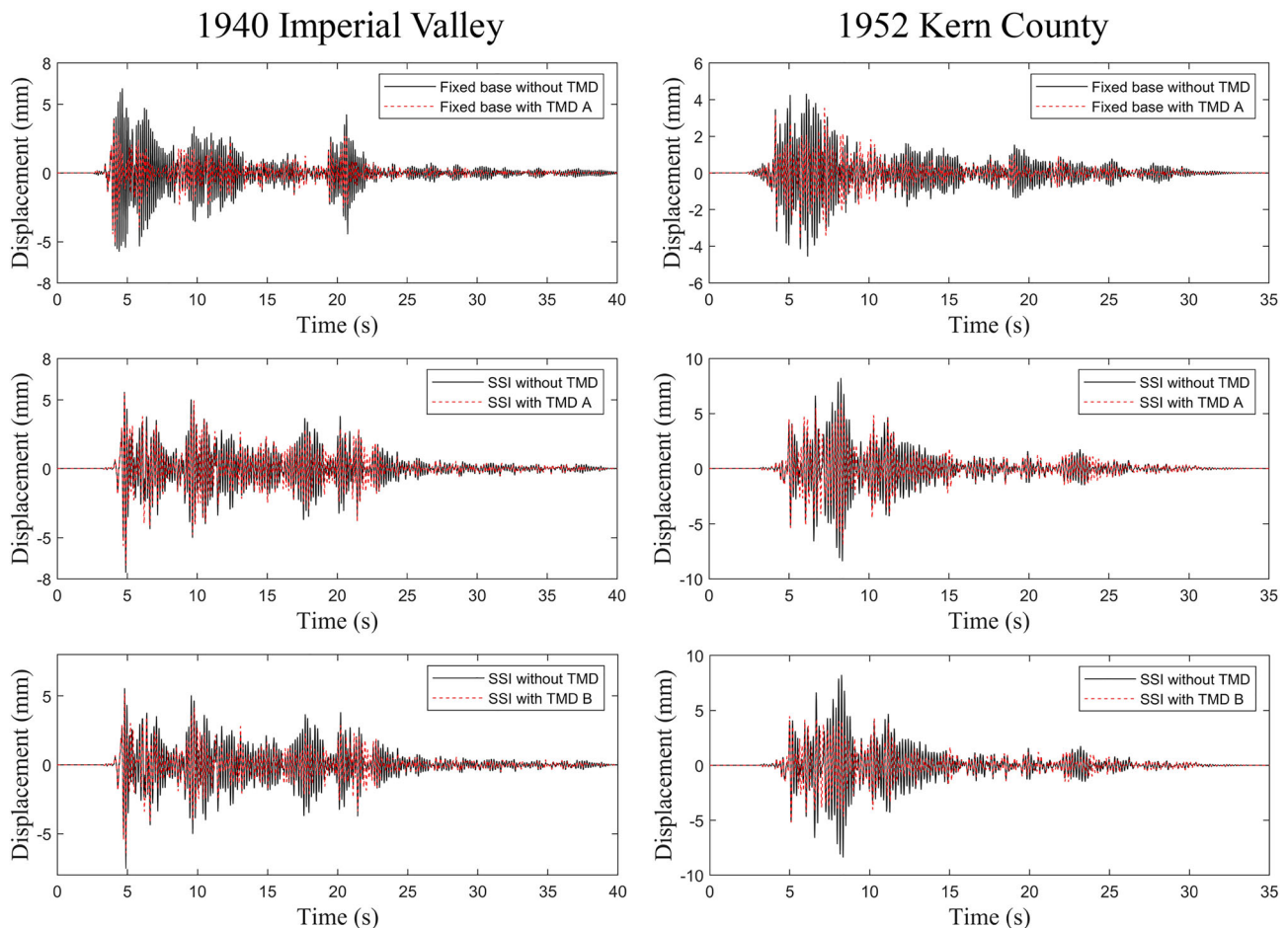

FIGURE 11 Displacement of the top of the wind turbine tower in different cases

	Imperial Valley 1940		Kern County 1952	
	Peak	RMS	Peak	RMS
Fixed-base with TMD A	17.74%	43.00%	21.74%	32.46%
SSI with TMD A	6.67%	10.91%	19.05%	15.38%
SSI with TMD B	14.67%	24.55%	38.10%	26.92%

and ground motion characteristics on the response reduction efficiency of TMD. Note that all TMDs used in this section are designed considering SSI, modeling the foundation with equivalent linear elastic springs and dashpots.

4.1 | Numerical model

The full-scale wind turbine described[36] was studied using the simplified finite element model presented in Section 3. The geometry and the material parameters of the tower and the foundation of the wind turbine tower are given in Section 2.1. The mass of the TMD is 5% of the total mass of the tower, the nacelle, and the blades. The frequency and the damping ratio of the TMD are determined by Equations 1 and 2 in Section 2.3, respectively. Three ground conditions are considered, namely, Classes C, D, and E according to the ASCE7-16,[46] which correspond to medium hard soil, soft soil, and extremely soft soil, respectively. ASCE7-16[46] describes the soil stiffness, defined by the ratio between the shear wave velocity (V_s) and the low-strain shear velocity (V_{s0}), as well as the soil hysteretic damping ratio β_0. These ratios depend on the earthquake intensity defined by the peak of the spectral acceleration of S_{DS}, shown in Table 9. Using Table 9, V_s and β_0 can be obtained by means of a linear interpolation with respect to S_{DS}.

In a preliminary analysis, the effect of the depth of soil from the foundation to the bedrock was found to be insignificant on the seismic response of both SSI systems, with and without TMD. Therefore, a constant soil depth of 12.8 m is used. The density and the Poisson's ratio of the soil are assumed to be 1800 kg/m^3 and 0.3, respectively. Mean shear wave velocity values of 560, 270, and 90 m/s are adopted to represent site Classes C, D, and E, respectively. In order to investigate the effect of site conditions on the response reduction efficiency of TMDs,

		Effective peak acceleration, $S_{DS}/2.5$			
Site class	V_{s0} (m/s)	$S_{DS}/2.5 = 0$	$S_{DS}/2.5 = 0.1$	$S_{DS}/2.5 = 0.4$	$S_{DS}/2.5 \geq 0.8$
C	360 ~ 760	1.00, 0.01	0.97, 0.01	0.87, 0.03	0.77, 0.05
D	180 ~ 360	1.00, 0.01	0.95, 0.02	0.71, 0.07	0.32, 0.15
E	<180	1.00, 0.01	0.77, 0.05	0.22, 0.20	0.22, 0.20

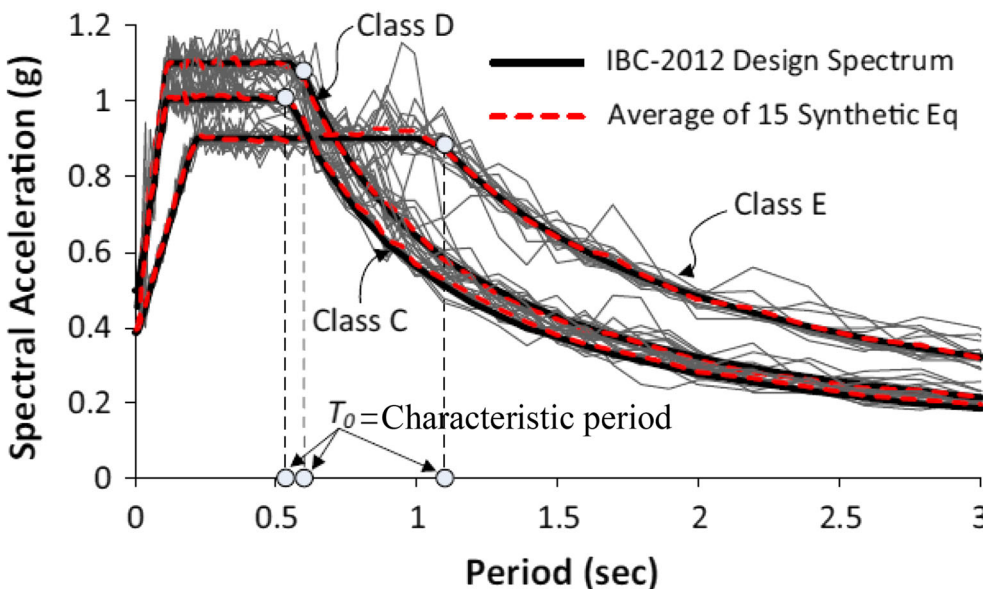Note: The values in the table are V_s/V_{s0} and β_0.

FIGURE 12   Comparison of the mean response spectra of 15 synthetic earthquakes with IBC-2012 code response spectra for site Classes C, D, and E

	Class C	Class D	Class E
Without TMD	0.5163	0.508	0.417
With TMD	0.4332	0.4263	0.351

three sets of spectrum-compatible synthetic accelerograms were used to represent the IBC-2012[47] design response spectra corresponding to soil Classes C, D, and E (see Figure 12). Each set of the synthetic earthquakes consists of 15 seismic excitations with a peak ground acceleration (PGA) of 0.4 g. These ground motions were generated artificially with a pseudo-random phasing and a time-varying modulating function[48] using SIMQKE,[49] and its average fits well with the design response spectrum (see Figure 12). In order to reach various earthquake intensity levels, the PGA of each ground motion was scaled from 0.1 to 1 g at 0.1-g intervals (i.e., total 10 different levels where considered). The fundamental frequency of the numerical model calculated from the NS is shown in Table 10, and it has a very good correlation with the measured value of 0.490 HZ on a stiff site.[36]

Four dimensionless parameters are defined to quantify the damping efficiency of TMD, including the peak acceleration ratio (PAR), the root mean square acceleration ratio (RAR), the peak displacement ratio (PDR), and the root mean square displacement ratio (RDR) given by Equations 13–16, respectively. The higher the values of PAR, RAR, PDR, and RDR, the lower the damping efficiency of the TMD.

$$PAR = \frac{\ddot{X}_{max,TMD}}{\ddot{X}_{max}},$$

(13)
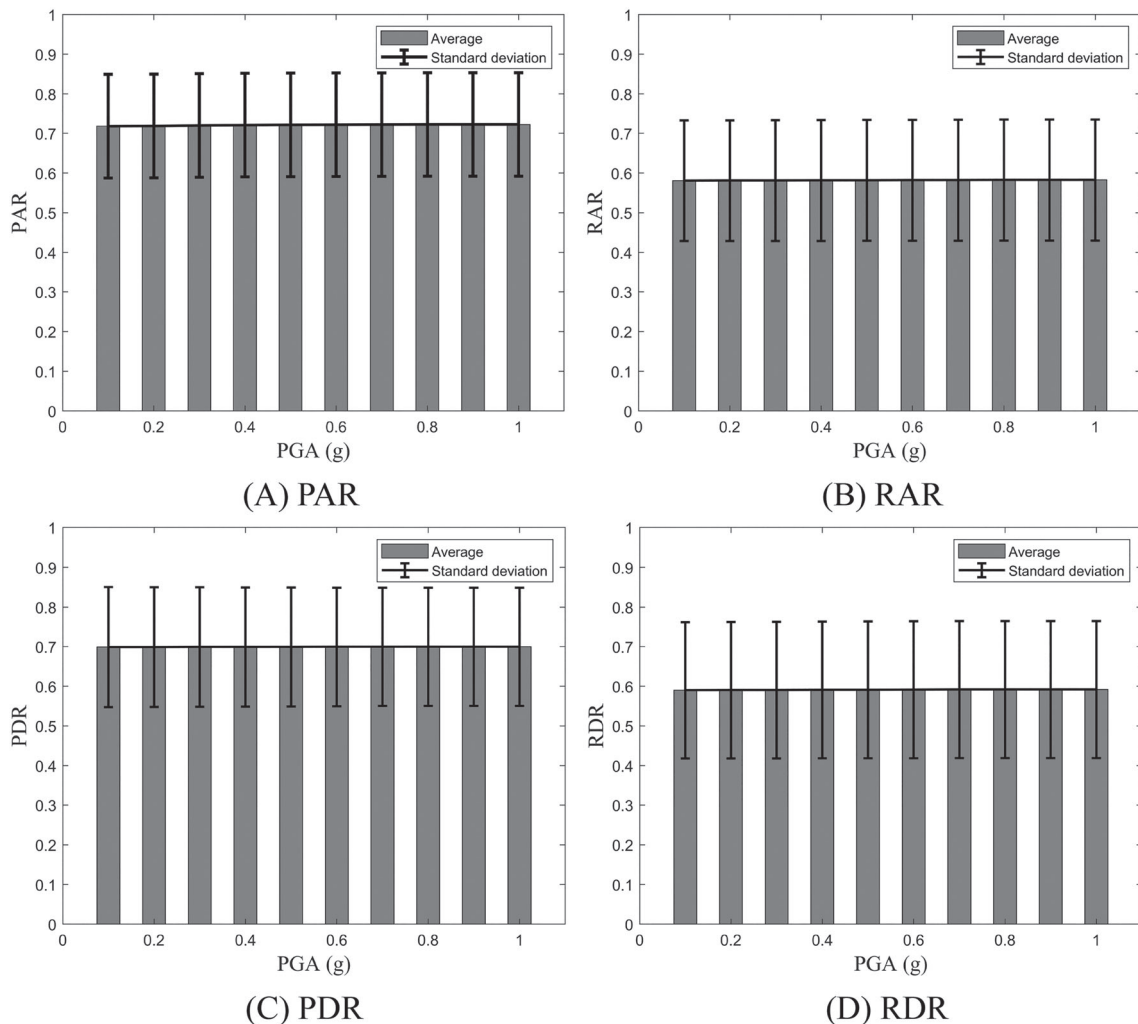
FIGURE 13 Variation of PAR, RAR, PDR, and RDR with PGA on site Class C
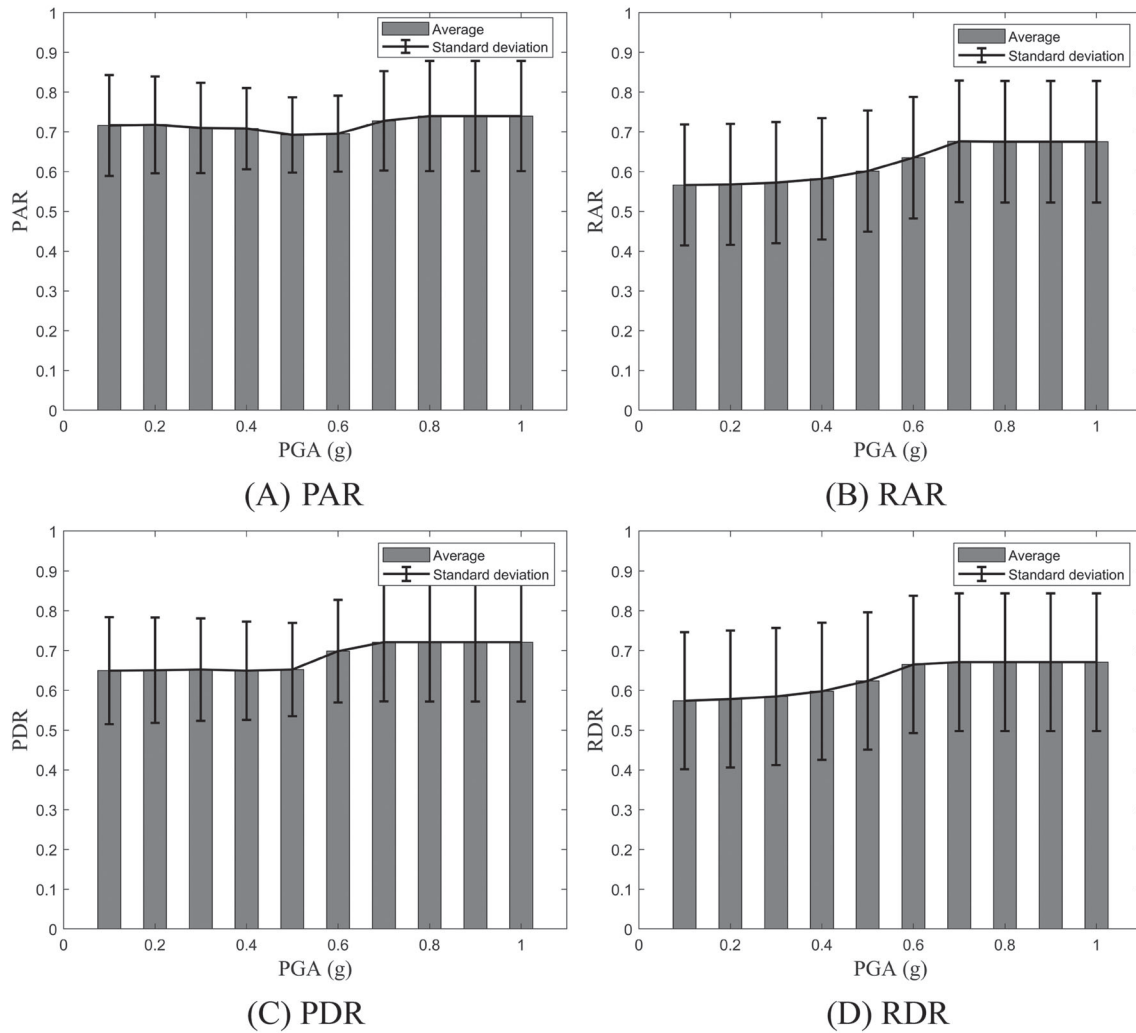
FIGURE 14 Variation of PAR, RAR, PDR, and RDR with PGA on site Class D

$$RAR = \frac{\ddot{X}_{RMS,TMD}}{\ddot{X}_{RMS}}, \tag{14}$$

$$PDR = \frac{X_{max,TMD}}{X_{max}}, \tag{15}$$

$$RDR = \frac{X_{RMS,TMD}}{X_{RMS}}, \tag{16}$$

where $\ddot{X}_{max,TMD}$ and $\ddot{X}_{max}$ represent the maximum absolute acceleration response of the top of the tower with and without TMD, respectively; $\ddot{X}_{RMS,TMD}$ and $\ddot{X}_{RMS}$ represent the RMS of absolute acceleration response of the top with and without TMD, respectively. Similarly, $X_{max,TMD}$ and X_{max} represent the maximum displacement (relative to the ground) of the tower top with and without TMD, respectively; $X_{RMS,TMD}$ and X_{RMS} represent the RMS of the stated displacements with and without TMD, respectively.

4.2 | Results and discussion

Figures 13–15 show the PAR, RAR, PDR, and RDR of the top of the wind turbine tower with and without TMD. The results include the arithmetic mean of each of the 15 synthetic records (represented by bars) and the corresponding standard deviation (represented by error bars).
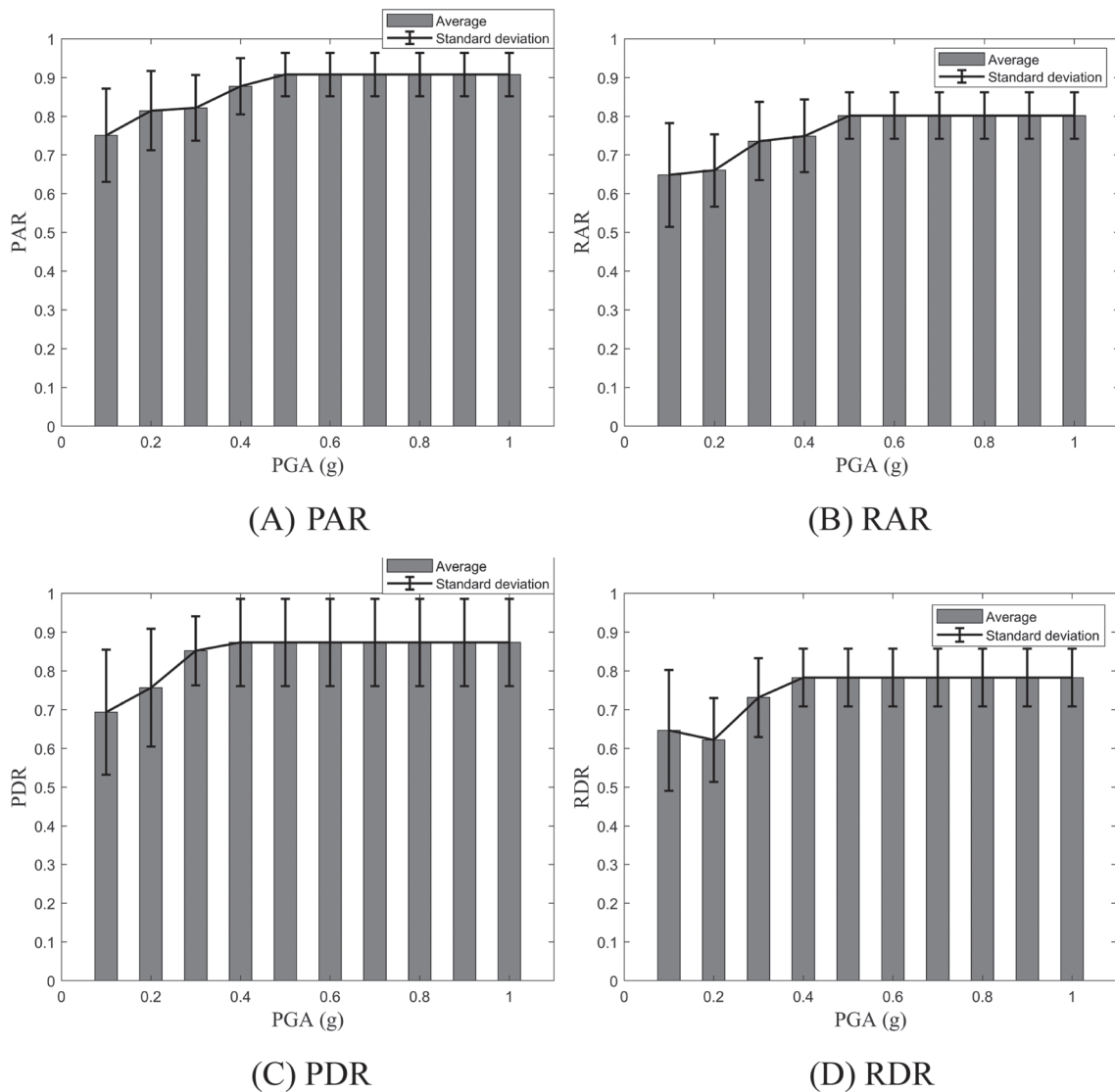
FIGURE 15 Variation of PAR, RAR, PDR, and RDR with PGA on site Class E

Figure 13 presents the results for the foundation site Class C (medium–hard soil). The average PAR (with the corresponding PDR results included between brackets in the following discussion) of the tower top increased from 0.718 (0.699) for a PGA of 0.1 g to 0.723 (0.700) for a PGA of 1 g, and the corresponding average RAR (RDR) increased from 0.581 (0.590) to 0.583 (0.592), respectively. Both the averaged and the individual results obtained for each record show that the efficiency of TMD is almost unaffected by the earthquake intensity. This can be explained by the fact that when the soil is competent, the damping provided by its interaction with the foundation is very small, and it is not influenced by the intensity of the earthquake motion.

Figures 14 shows that on site Class D (soft soil), the average PAR (PDR) decreases slightly from 0.716 (0.650) for a PGA of 0.1 g to 0.692 for a PGA of 0.5 g and then it rises to 0.740 (0.721) when PGA is above 0.8 g (0.7 g), while the mean RAR (RDR) increases monotonically by increasing the PGA up to 0.675 (0.671). The results show that the influence of the earthquake intensity is significant when the soil surrounding the foundation is relatively soft (Class D), and in this case, efficiency of the TMD tends to decrease by increasing the earthquake intensity. This is remarkable since in this study, damage-induced detuning effects are not considered.

Figure 15 shows the results corresponding to site Class E (very soft soil). The average PAR (PDR) increases from 0.751 (0.693) for a PGA of 0.1 g to 0.908 (0.873) when PGA ≥ 0.5 g (0.4 g), whereas the maximum mean RAR (RDR) is around 0.8 (0.78). It shows that the site Class E soil provides a large amount of damping, which contributes more to the reduction of the structural response than the TMD. In this case, the TMDs are not as efficient as they are when the foundation of the tower is on stiffer soils. In soft soils, the response reduction efficiency of the TMD decreases by increasing the earthquake intensity because the dissipation introduced by the damping of the soil also increases.
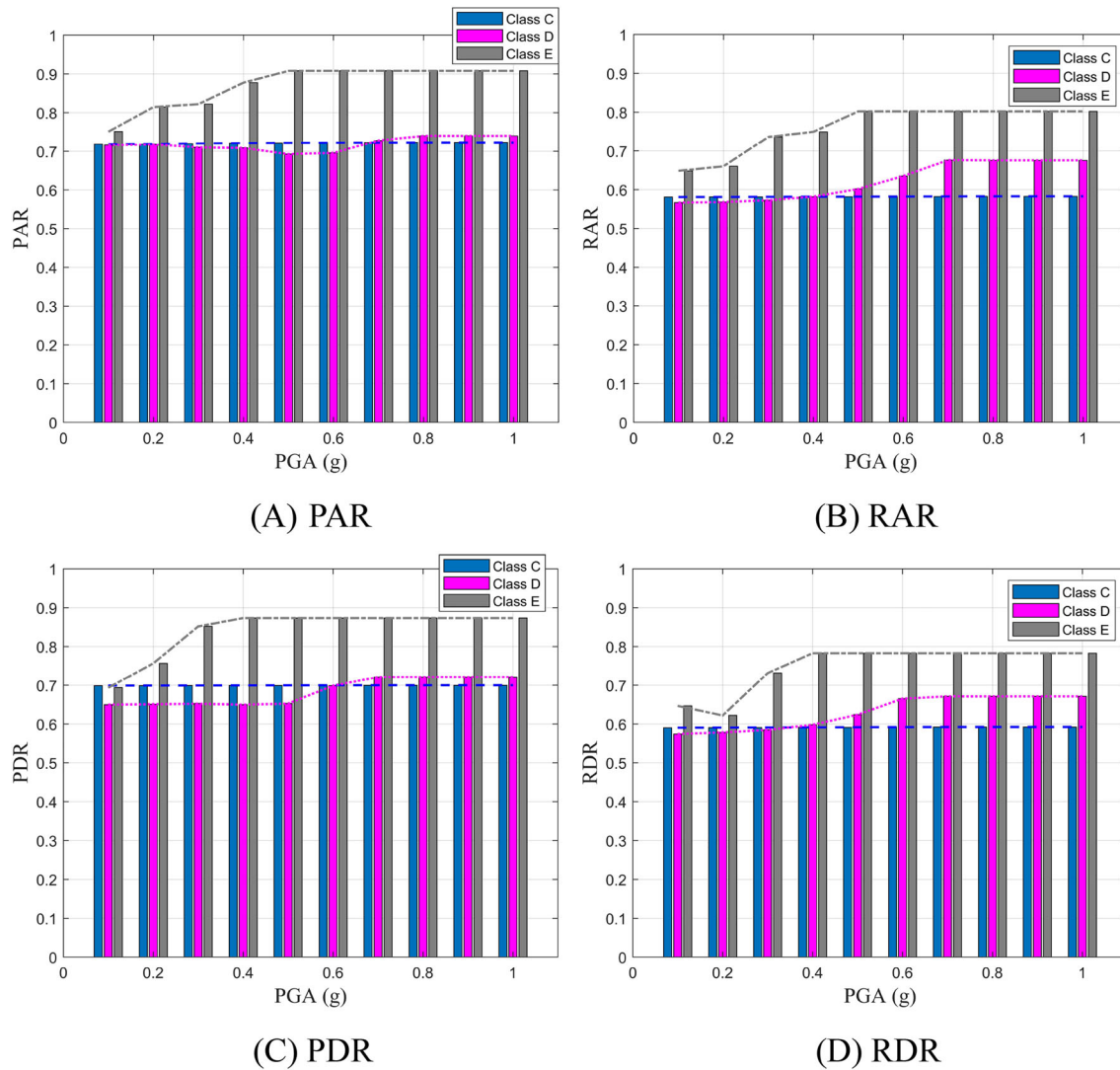
FIGURE 16 Variation of the average PAR, RAR, PDR, and RDR with PGA on site Classes C, D and E

When the earthquake intensity is large enough, PAR, RAR, PDR, and RDR remain constant. This is because in Table 9, when $S_{DS}/2.5$ is larger than 0.8 for site Classes C and D, or larger than 0.4 for site Class E, the shear wave velocity ratio and the damping ratio of the soil do not change. Figures 13–15 also show large scatter of the PAR, RAR, PDR, and RDR for different ground motions, indicating the variability of the response reduction efficiency of TMD with respect to the ground motion, even considering artificial earthquakes with very small record-to-record variability.

Figure 16 shows the arithmetic average of the PAR, RAR, PDR, and RDR for all records in the three site conditions. The TMD response reduction efficiency on site Class C is less than that on site Class D over a certain range of PGA values in both Figure 16A,B, which contradicts the accepted understanding that the softer the soil, the lower the TMD efficiency. This may be due to the fact that the characteristics of the ground motion used for the site Class C are different from those corresponding to the site Class D. To explore this effect, Figure 17 presents the results for the ground motions corresponding to a single site class (site Class C). In this figure, it is observed that the results of PAR, RAR, PDR, and RDR would show higher values on softer site classes. Therefore, it is concluded that the response reduction efficiency of TMD depends not only on the soil stiffness but also on the shape of the response spectra of the ground motions, both of which are affected by the site classes and earthquake intensity levels. Figure 16 can be used for rational selection of TMD considering SSI. It should be noted that the SSI model is based on an equivalent-linear material assumption, whereas at high levels of PGA, damage may occur to the system. In this case, the effective frequency of vibration of the system becomes lower, and the frequency of the TMDs, which were tuned to the undamaged system, would be different from the effective frequency. In addition, the inelastic energy dissipation would far exceed that due to the damping of the TMD. This means that it is meaningless to discuss the TMD effects at very high PGA levels. Therefore, the above discussion is applicable to low-to-intermediate PGA levels discussed here in this section (e.g., PGA < 0.5 g).
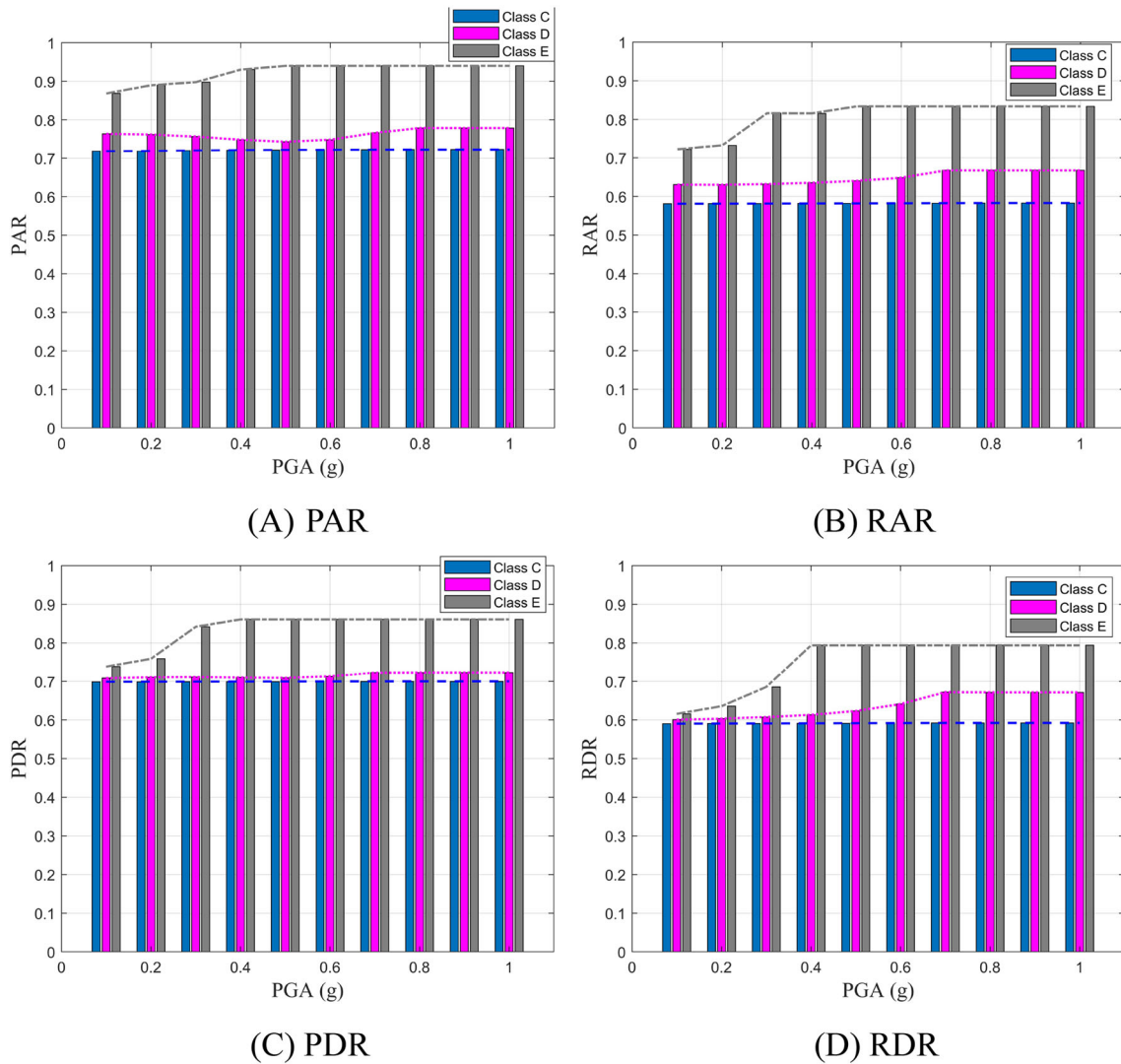
FIGURE 17 Average PAR, RAR, PDR, and RDR using ground motions compatible with site Class C

5 | CONCLUSIONS

In this paper, a series of shaking table tests were conducted for a small-scale wind turbine model with TMD designed with and without considering SSI. The results verified that the TMD considering SSI was more efficient suppressing the vibrations of the structure. A simplified model of a wind turbine tower with TMD considering SSI under earthquake action was established. Using the simplified analysis model proposed in this paper, the comparison between the calculation results and the shaking table test validates the model. The effect of site and earthquake intensity on the response reduction efficiency of TMDs was discussed with NS under synthetic ground motions generated for three different types of foundation soil. In general, the softer the site soil and the larger the earthquake intensity results in lower TMD efficiency, but there are exceptions. This is due to the fact that the vibration control of TMDs depends not only on the soil stiffness but also on the frequency content of the ground motions, both of which are affected by the site classes and by the earthquake intensity levels. Moreover, the PAR, RAR, PDR, and RDR of the top of the wind turbine tower with and without TMD for different earthquake intensities and sites were suggested to help in the selection of effective TMDs considering the foundation soil conditions.

ORCID

Yang Lu https://orcid.org/0000-0002-6091-1231

REFERENCES

1. World Wind Energy Association (WWEA). https://wwindea.org/blog/2019/02/25/wind-power-capacity-worldwide-reaches-600-gw-539-gw-added-in-2018/
2. Bazeos N, Hatzigeorgiou G, Hondros I, Karamaneas H, Karabalis D, Beskos D. Static, seismic and stability analyses of a prototype wind turbine steel tower. *Eng Struct*. 2002;24(8):1015-1025.
3. Lavassas I, Nikolaidis G, Zervas P, Efthimiou E, Doudoumis IN, Baniotopoulos CC. Analysis and design of the prototype of a steel 1-MW wind turbine tower. *Eng Struct*. 2003;25(8):1097-1106.
4. Prowell I, Veletzos M, Elgamal A, Restrepo J. Experimental and numerical seismic response of a 65kW wind turbine. *J Earthquake Eng*. 2009;13(8):1172-1190.
5. Dai K, Bergot A, Liang C, Xiang W-N. Environmental issues associated with wind energy—a review. *Renew Energy*. 2015;75:911-921.
6. IEC 61400-1 Wind Turbines-Part 1: design requirements. Geneva, Switzerland: International Electrotechnical Commission (IEC), 2005.
7. *Guidelines for Certification of Offshore Wind Turbines*. Hamburg, Germany: Germanischer Lloyd (GL); 2003.
8. Chou JS, Tu WT. Failure analysis and risk management of a collapsed large wind turbine tower. *Eng Fail Anal*. 2011;18(1):295-313.
9. Dai K, Sheng C, Zhao Z, Yi Z, Camara A, Bitsuamlak G. Nonlinear response history analysis and collapse mode study of a wind turbine tower subjected to cyclonic winds. *Wind Struct*. 2017;25(1):79-100.
10. Rahman M, Ong ZC, Chong WT, Julai S, Khoo SY. Performance enhancement of wind turbine systems with vibration control: a review. *Renew Sustain Energy Rev*. 2015;51:43-54.
11. Murtagh PJ, Ghosh A, Basu B, Broderick BM. Passive control of wind turbine vibrations including blade/tower interaction and rotationally sampled turbulence. *Wind Energy*. 2008;11(4):305-317.
12. Lackner MA, Rotea MA. Passive structural control of offshore wind turbines. *Wind Energy*. 2011;14(3):373-388.
13. Stewart G, Lackner M. Offshore wind turbine load reduction employing optimal passive tuned mass damping systems. *IEEE Trans Contr Syst Tech*. 2013;21(4):1090-1104.
14. Ghaemmaghami A, Kianoush R, Yuan XX. Numerical modeling of dynamic behavior of annular tuned liquid dampers for applications in wind towers. *Comput Aided Civ Inf Eng*. 2013;28(1):38-51.
15. Chen J, Zhan G, Zhao Y. Application of spherical tuned liquid damper in vibration control of wind turbine due to earthquake excitations. *Struct Design Tall Spec Build*. 2016;25(10):431-443.
16. Colwell S, Basu B. Tuned liquid column dampers in offshore wind turbines for structural control. *Eng Struct*. 2009;31(2):358-368.
17. Mensah AF, Dueñas-Osorio L. Improved reliability of wind turbine towers with tuned liquid column dampers (TLCDs). *Struct Saf*. 2014;47:78-86.
18. Chen J, Liu Y, Bai X. Shaking table test and numerical analysis of offshore wind turbine tower systems controlled by TLCD. *Earthquake Eng Eng Vib*. 2015;14(1):55-75.
19. Chen J, Georgakis CT. Tuned rolling-ball dampers for vibration control in wind turbines. *J Sound Vib*. 2013;332(21):5271-5282.
20. Zhang ZL, Chen JB, Li J. Theoretical study and experimental verification of vibration control of offshore wind turbines by a ball vibration absorber. *Struct Infrastruct Eng*. 2014;10(8):1087-1100.
21. Zuo H, Bi K, Hao H. Using multiple tuned mass dampers to control offshore wind turbine vibrations under multiple hazards. *Eng Struct*. 2017;141:303-315.
22. Stewart GM, Lackner MA. The effect of actuator dynamics on active structural control of offshore wind turbines. *Eng Struct*. 2011;33(5):1807-1816.
23. Caterino N. Semi-active control of a wind turbine via magnetorheological dampers. *J Sound Vib*. 2015;345:1-17.
24. Zhao Z, Dai K, Lalonde ER, et al. Studies on application of scissor-jack braced viscous damper system in wind turbines under seismic and wind loads. *Engineering Structures*. 2019;196:109294. https://doi.org/10.1016/j.engstruct.2019.109294
25. Zhang R, Zhao Z, Dai K. Seismic response mitigation of a wind turbine tower using a tuned parallel inerter mass system. *Eng Struct*. 2019;180:29-39.
26. Katsanos EI, Thöns S, Georgakis CT. Wind turbines and seismic hazard: a state-of-the-art review. *Wind Energy*. 2016;19(11):2113-2133.
27. Zhao X, Maisser P. Seismic response analysis of wind turbine towers including soil-structure interaction. *Proc Institution Mech Eng Part K: J Multi-body Dyn*. 2006;220(1):53-61.
28. Andersen LV, Vahdatirad MJ, Sichani MT, Sørensen JD. Natural frequencies of wind turbines on monopile foundations in clayey soils—a probabilistic approach. *Comput Geotech*. 2012;43:1-11.
29. Arany L, Bhattacharya S, Macdonald JHG, Hogan SJ. Closed form solution of Eigen frequency of monopile supported offshore wind turbines in deeper waters incorporating stiffness of substructure and SSI. *Soil Dynam Earthquake Eng*. 2016;83:18-32.
30. Lombardi D, Bhattacharya S, Wood DM. Dynamic soil–structure interaction of monopile supported wind turbines in cohesive soil. *Soil Dynam Earthquake Eng*. 2013;49:165-180.
31. Bhattacharya S, Adhikari S. Experimental validation of soil–structure interaction of offshore wind turbines. *Soil Dynam Earthquake Eng*. 2011;31(5-6):805-816.
32. Harte M, Basu B, Nielsen SRK. Dynamic analysis of wind turbines including soil-structure interaction. *Eng Struct*. 2012;45:509-518.
33. Kim DH, Lee SG, Lee IK. Seismic fragility analysis of 5 MW offshore wind turbine. *Renew Energy*. 2014;65:250-256.
34. *BS EN 206 Concrete-Part 1: Specification, Performance, Production and Conformity*. Brussels, Belgium: European committee for standardization (CEN); 2013.
35. Zhou Y, Lu X. *Method and Technology for Shaking Table Model Test of Building Structures*. Beijing: Science Press; 2012.

36. Dai K, Huang Y, Gong C, Huang Z, Ren X. Rapid seismic analysis methodology for in-service wind turbine towers. *Earthquake Eng Eng Vib*. 2015;14(3): 539-548.

37. Dai K, Wang Y, Huang Y, Zhu W, Xu Y. Development of a modified stochastic subspace identification method for rapid structural assessment of in-service utility-scale wind turbine towers. *Wind Energy*. 2017;20(10):1687-1710.

38. Lu X, Li P, Chen B, Chen Y. Computer simulation of the dynamic layered soil pile structure interaction system. *Canadian Geotech J*. 2005;42(3): 742-751.

39. Shang S, Liu F, Lu H, Du Y. Design and experimental study of a model soil used for shaking table test. *Earthquake Eng Eng Vib*. 2006;26(4):199-204.

40. Yan X, Yuan J, Yu H, Bobet A, Yuan Y. Multi-point shaking table test design for long tunnels under non-uniform seismic loading. *Tunnel Underground Space Technol*. 2016;59:114-126.

41. Tsai H-C, Lin G-C. Optimum tuned-mass dampers for minimizing steady-state response of support-excited and damped systems. *Earthq Eng Struct Dyn*. 1993;22(11):957-973.

42. Sodano HA, Bae JS, Inman DJ, Keith Belvin W. Concept and model of eddy current damper for vibration suppression of a beam. *J Sound Vib*. 2005; 288(4–5):1177-1196.

43. Ancheta TD, Darragh RB, Stewart JP, et al. PEER NGA-West2 Database. Pacific Earthquake Engineering Research Center

44. Du B, Xiang H, Ge Y, Zhu L. Derivation and application of 3D-Beam's element stiffness and mass matrix with shear effect. *J Chongqing Jiaotong Univ*. 2008;4:502-507.

45. Gazetas G. Foundation Vibrations. In: Fang H-Y, ed. *Foundation Engineering Handbook*. 2nd ed. Boston, MA, USA: Springer; 1991:553-593.

46. ASCE/SEI 7-16. *Minimum Design Loads for Buildings and Other Structures*. Reston, Virginia: American Society of Civil Engineers; 2017.

47. IBC. *International Building Code. IBC-2012*. Country Club Hills, USA: International Code Council, INC; 2012.

48. Lu Y, Hajirasouliha I, Marshall AM. Performance-based seismic design of flexible-base multi-storey buildings considering soil–structure interaction. *Eng Struct*. 2016;108:90-103.

49. Gasparini DA, Vanmarcke E. *SIMQKE: a Program for Artificial Motion Generation: User's Manual and Documentation*. Cambridge, MA: MIT Department of Civil Engineering; 1976.

APPENDIX A.

The shear-deformable element stiffness matrix $[K_e]$ is as follows:

$$[K_e] = \begin{bmatrix} \dfrac{12EI}{(1+\Phi)l^3} & \dfrac{6EI}{(1+\Phi)l^2} & \dfrac{-12EI}{(1+\Phi)l^3} & \dfrac{6EI}{(1+\Phi)l^2} \\ \dfrac{6EI}{(1+\Phi)l^2} & \dfrac{(4+\Phi)EI}{(1+\Phi)l} & \dfrac{-6EI}{(1+\Phi)l^2} & \dfrac{(2-\Phi)EI}{(1+\Phi)l} \\ \dfrac{-12EI}{(1+\Phi)l^3} & \dfrac{-6EI}{(1+\Phi)l^2} & \dfrac{12EI}{(1+\Phi)l^3} & \dfrac{-6EI}{(1+\Phi)l^2} \\ \dfrac{6EI}{(1+\Phi)l^2} & \dfrac{(2-\Phi)EI}{(1+\Phi)l} & \dfrac{-6EI}{(1+\Phi)l^2} & \dfrac{(4+\Phi)EI}{(1+\Phi)l} \end{bmatrix}, \tag{A1}$$

where $\Phi = (12EI)/(GAl^2) = (12Ek_y)/(GAl^2)$, ($I$ is the inertia; A is the sectional area; k_y is shear coefficient; l is element length).

The consistent element mass matrix $[M_e]$ is as follows:

$$[M_e] = \rho Al \begin{bmatrix} A_z & C_z & B_z & -D_z \\ C_z & E_z & D_z & F_z \\ B_z & D_z & A_z & -C_z \\ -D_z & F_z & -C_z & E_z \end{bmatrix}, \tag{A2}$$

in which,

$$A_z = \frac{\frac{13}{35} + \frac{7}{10}\Phi + \frac{1}{3}\Phi^2 + \frac{6}{5}(r/l)^2}{(1+\Phi)^2}, \tag{A3}$$

$$B_z = \frac{\frac{9}{70} + \frac{3}{10}\Phi + \frac{1}{6}\Phi^2 - \frac{6}{5}(r/l)^2}{(1+\Phi)^2}, \tag{A4}$$

$$C_z = \frac{\left[\frac{11}{210} + \frac{11}{120}\Phi + \frac{1}{24}\Phi^2 + \left(\frac{1}{10} - \frac{1}{2}\Phi\right)\left(\frac{r}{l}\right)^2\right]l}{(1+\Phi)^2}, \tag{A5}$$

$$D_z = \frac{\left[\frac{13}{420} + \frac{3}{40}\Phi + \frac{1}{24}\Phi^2 - \left(\frac{1}{10} - \frac{1}{2}\Phi\right)\left(\frac{r}{l}\right)^2\right]l}{(1+\Phi)^2}, \tag{A6}$$

$$E_z = \frac{\left[\frac{1}{105} + \frac{1}{60}\Phi + \frac{1}{120}\Phi^2 + \left(\frac{2}{15} + \frac{1}{6}\Phi + \frac{1}{3}\Phi^2\right)\left(\frac{r}{l}\right)^2\right]l^2}{(1+\Phi)^2}, \tag{A7}$$

$$F_z = \frac{-\left[\frac{1}{140} + \frac{1}{60}\Phi + \frac{1}{120}\Phi^2 + \left(\frac{1}{30} + \frac{1}{6}\Phi - \frac{1}{6}\Phi^2\right)\left(\frac{r}{l}\right)^2\right]l^2}{(1+\Phi)^2}, \tag{A8}$$

where $r = \sqrt{I/A}$ represents the radius of rotation around the midpoint of the section.

The stiffness and mass matrices are defined by the DOFs according to the element displacement vector given in Equation A9 and sketched in Figure A1.

$$u_e = \begin{bmatrix} w_i & \theta_i & w_j & \theta_j \end{bmatrix}^T, \tag{A9}$$

where w_i and w_j represent the horizontal translation of nodes i and j, respectively; θ_i and θ_j represent the rotation at nodes i and j, respectively.

FIGURE A1   Schematic diagram of element displacement vector